ACS Photonics

Letter

pubs.acs.org/journal/apchd5

Sudden, Laser-Induced Heating through Silicon Nanopatterning

Roshni Biswas and Michelle L. Povinelli*

Ming Hsieh Department of Electrical Engineering, University of Southern California, Los Angeles, California 90089, United States

ABSTRACT: We introduce a nanoheater structure based on laser illumination of a nanopatterned silicon membrane. We develop a model to predict the time-dependent temperature rise. Simulations show a temperature rise that is much larger and more sudden than in an unpatterned membrane. This effect is attributed to resonantly enhanced heating. We fabricate a prototype device and observe the signature of sudden heating in the optical transmission response.

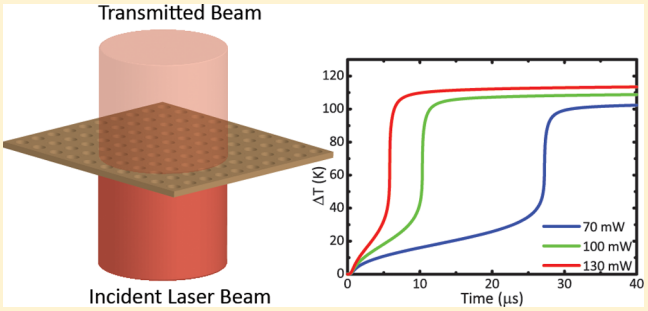

KEYWORDS: *photothermal effects, photonic crystals, thermo-optic nonlinearity, plasmonic heating, coupled mode theory, finite element methods*

Laser-induced heating is a versatile technique for the remote heating of objects on the nanoscale. Past work has investigated the use of plasmonic nanoparticles as nanoheaters.[1] Near the plasmon resonance wavelength, the optical absorption of the nanoparticle is high, allowing efficient conversion of laser light to heat.[2−4] This effect has been exploited for diverse applications including optofluidics,[5,6] vapor generation,[7] photothermal therapies,[8,9] and DNA melting analysis.[10] The absorption strength at resonance can be further increased using a gold nanoparticle array.[11,12] Nanoparticle array heaters,[13,14] which are amenable to lab-on-a-chip experiments, have found application in catalyzing chemical reactions,[15] growth of nanowires,[16] manipulating cell adhesion,[17] and controlling microfluidic mixing.[18]

Here we propose an alternate mechanism for nanoscale heat generation that does not require plasmonic materials. Our approach uses a nanopatterned, all-silicon platform to create a novel nanoheater. The nanoheater exhibits sudden, rapid heating with a tunable onset time that can be controlled via laser power. Operation is compatible with laser wavelengths in the 800−1100 nm range, overlapping the biological transparency window.[19] Moreover, our nanoheater device is made via a CMOS-compatible microfabrication process, enabling low-cost application.

We design a highly absorptive optical mode in silicon by starting with a thin membrane and etching a 2D array of holes. This device, known as a photonic-crystal slab, supports optical resonance modes.[20,21] By choosing the hole spacing and diameter appropriately, we can create resonances in a desired wavelength range. When the incident laser wavelength coincides with a resonance, the absorption is greatly enhanced.[22] In previous work, we have measured the transmission of laser light through the device and showed that it is highly nonlinear with laser power.[23] We attributed the nonlinearity to absorptive heating.[23] In this work, we introduce a coupled thermo-optical model to predict the temperature rise in the device. We find that the temperature rises suddenly and rapidly with time. The sudden heating is signaled by a large jump in laser transmission. We fabricate a prototype device and measure the time-dependent transmission at a laser wavelength of 976 nm. Our experimental results confirm the sudden jump predicted by simulation and indicate a >168 K temperature rise at steady state given a 127 mW incident laser beam with 10 μm spot size.

We consider light normally incident on a silicon photonic-crystal slab, as shown in Figure 1a. For concreteness, we set the slab thickness to 340 nm, the lattice constant to 470 nm, and the hole diameter to 160 nm. We simulate the transmission spectrum using the finite-difference time domain (FDTD) method (Lumerical). The transmission spectrum is shown in Figure 1b and has a Fano line shape. The characteristic line shape results from interference between Fabry−Perot reflections and a guided resonance mode in the slab.[20] The absorption spectrum is shown in Figure 1c and has a Lorentzian shape. In contrast, the transmission and absorption spectra of an unpatterned silicon slab with the same thickness are shown in Figure 1d and e. They are both relatively featureless within the wavelength range shown. At resonance, the absorption of the photonic-crystal slab is 94 times higher than the unpatterned slab.

We model the coupled thermal and optical response of the system using the transient 3D heat equation in combination with coupled mode theory. The temperature T of the photonic-crystal slab is governed by

$$\rho C_p \frac{\partial T}{\partial t} = \nabla(k\nabla T) + P_{\text{abs}}(t) \tag{1}$$

Received: September 15, 2015
Published: November 25, 2015

DOI: 10.1021/acsphotonics.5b00521
ACS Photonics 2015, 2, 1681−1685

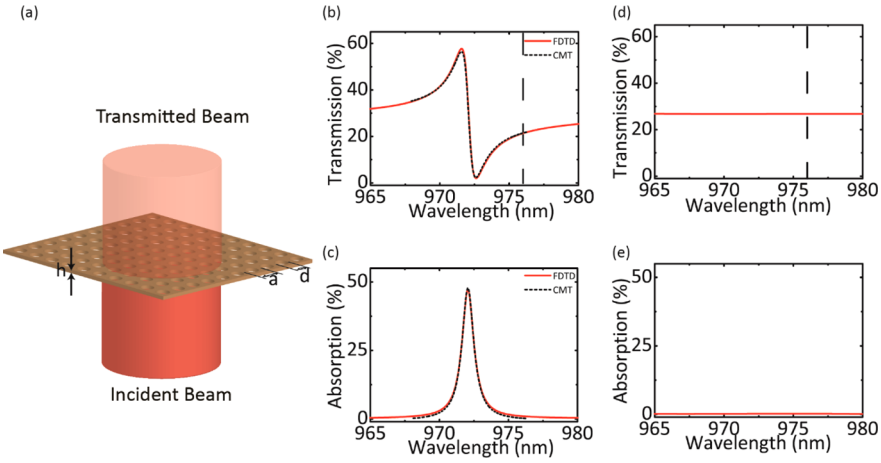

Figure 1. (a) Schematic of a photonic-crystal slab (a = 470 nm, d = 160 nm, and h = 340 nm) illuminated normally by a plane wave. (b) Transmission and (c) absorption of the photonic-crystal slab; (d) transmission and (e) absorption of an unpatterned slab. The dotted lines on the transmission plots show the position of the laser wavelength used in simulations.

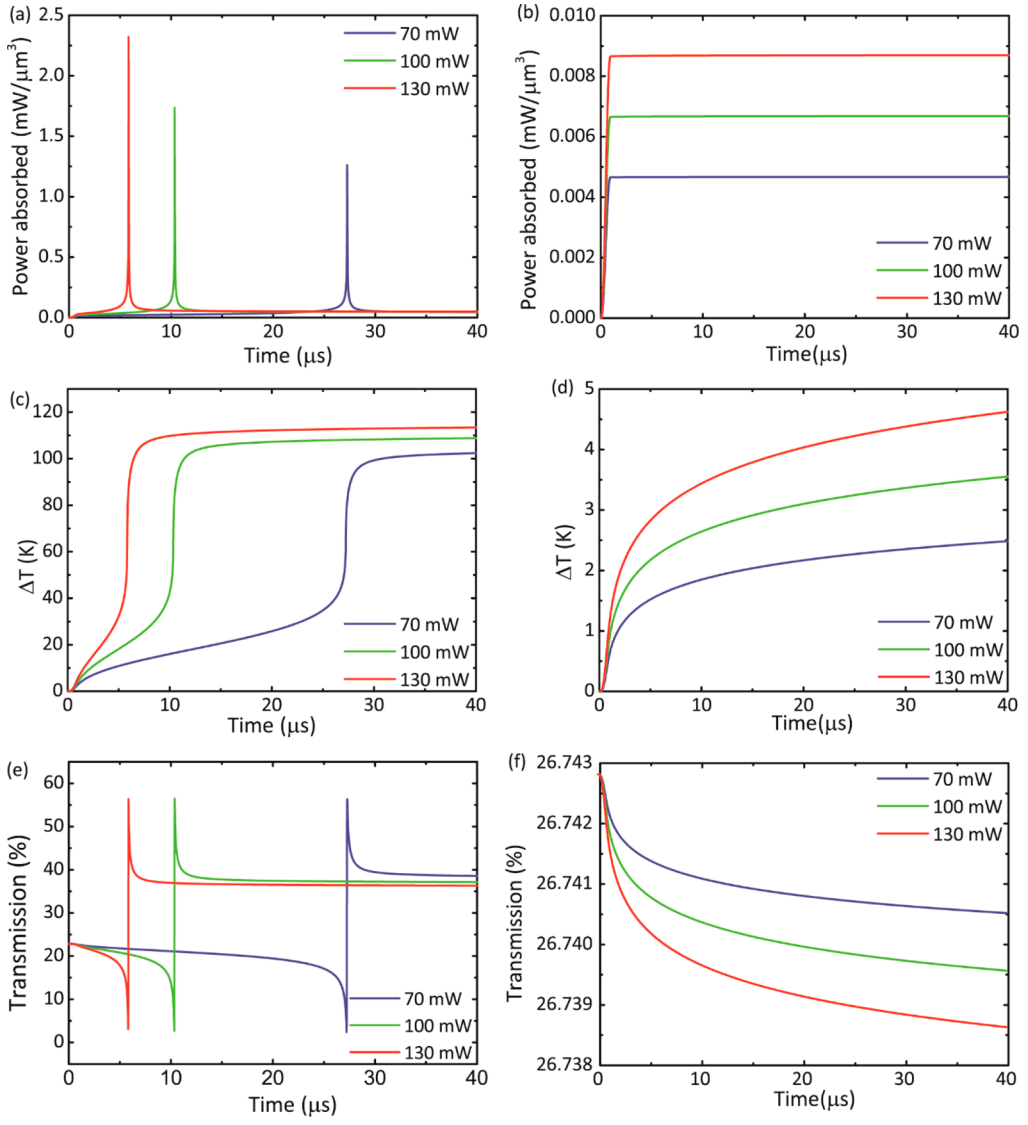

Figure 2. Left and right columns denote the photonic-crystal slab and unpatterned silicon slab, respectively: (a, b) absorbed power; (c, d) temperature variation; (e, f) transmission as a function of time.

DOI: 10.1021/acsphotonics.5b00521
ACS Photonics 2015, 2, 1681−1685

where ρ, C_p, and k represent the density, heat capacity, and thermal conductivity of the slab, respectively. The absorbed power P_{abs} can be determined from coupled mode theory:[24]

$$P_{abs}(t) = P_{in}\frac{2\gamma_i\gamma_r}{(\omega_{op} - \omega_o'(t))^2 + (\gamma_i + \gamma_r)^2} \quad (2)$$

where P_{in} denotes the power of the input laser pulse, ω_o is the operating frequency of the laser, γ_r is the decay rate of the resonance due to radiation loss, and γ_i is the decay rate due to material absorption loss. The frequency of the guided resonance mode, $\omega_o'(t)$, depends on the time-dependent temperature of the slab:

$$\omega_o'(t) = \omega_o - \frac{\omega_o}{n_0}\frac{dn}{dT}(T(t) - T_0) \quad (3)$$

where ω_o is the initial frequency of the guided resonance mode (e.g., the frequency at room temperature, in the absence of laser heating), dn/dT is the thermo-optic coefficient of silicon, and n_0 is the refractive index at room temperature (T_0). Equations 1 through 3 form a set of coupled equations that can be solved self-consistently for $T(t)$, $\omega_o'(t)$, and $P_{abs}(t)$, given the parameters ω_o, γ_i, and γ_r. The solution allows the calculation of the transmission line shape:[25]

$$T_{trans}(t) = \frac{(t_s\gamma_i)^2 + (t_s(\omega_{op} - \omega_o'(t)) + r_s\gamma_r)^2}{(\omega_{op} - \omega_o'(t))^2 + (\gamma_r + \gamma_i)^2} \quad (4)$$

where t_s and r_s are the direct transmission and reflection coefficients.

To determine the parameter values, we perform a fit of the coupled mode theory to the FDTD spectrum. For simplicity, we first consider a lossless ($\gamma_i = 0$), nondispersive medium for the slab in the limit of low incident power. Then the transmission line shape takes the simplified form

$$T = \frac{(t_s(\omega - \omega_o) + r_s\gamma_r)^2}{(\omega - \omega_o)^2 + \gamma_r^2} \quad (5)$$

A fit to the lossless FDTD result yielded values of $t_s = 0.534$, $r_s = 0.859$, $\omega_o = 1939.13$ THz, and $\gamma_r = 0.618$ THz. We obtain γ_i assuming direct absorption effects only, neglecting absorption due to two-photon processes or free carrier effects. Then $\gamma_i = (\omega k/n)\xi$, where n is the real part of the refractive index, k is the imaginary part, and ξ is the fraction of the modal volume contained in the dielectric.[26] The value obtained for γ_i was 0.417 THz. The fit to the spectrum using the parameter values is shown in Figure 1b and shows excellent agreement with the FDTD result.

We used the finite element method (COMSOL) to solve for the transient heating response. We simulated an axisymmetric structure consisting of a silicon disk of thickness 340 nm with a radius of 0.5 mm. We took the top and bottom surfaces of the disk to be thermally insulated, approximating a silicon disk in air. The lateral surface of the structure (side walls of the disk) is fixed at room temperature. A heat source with a Gaussian spatial profile (full width at half maximum of 10 μm) is positioned at the center of the disk. The product of the density and heat capacity terms in eq 1 is set by multiplying the values for bulk silicon with the volume fill fraction (0.91) of the photonic-crystal slab. To approximately model the effect of the holes on the thermal conductivity, we assumed a value of thermal conductivity (50 W/m·K) that lies between that of bulk silicon (130 W/m·K) and values reported in the literature for holey silicon membranes (1.73 W/m·K)[27] with higher air filling fractions.

The results of the FEM simulations are illustrated in Figure 2. We assumed a laser wavelength of 976 nm (dashed line in Figure 1a), detuned by 4 nm above the initial position of the resonance. The laser is turned on smoothly over 1 μs. Looking first at the 70 mW curve in Figure 2a (blue line), the absorbed power shows a sharply peaked response as a function of time. Increasing the laser power (green and red lines) decreases the response time: the absorption peak in Figure 2a moves to shorter times. This behavior is in contrast to the unpatterned slab, for which the absorption is low and constant after laser turn on (Figure 2b). The absorption peak in the photonic-crystal slab corresponds to a temperature jump, shown in Figure 2c. The sudden, rapid change in temperature at maximum absorption is in contrast to the unpatterned slab, for which the temperature rise is low (4.62 K) and smooth (Figure 2d). The transmission spectrum of the photonic-crystal slab (Figure 2e) shows a signature of the sudden temperature rise of the photonic-crystal slab. The spectrum has an asymmetric Fano shape in time, with a large transmission jump from about ∼1% to ∼58% that coincides with the temperature jump in Figure 2c.

The large, sudden heating observed in the photonic-crystal slab arises from optical resonance effects. When the laser is initially turned on, light is absorbed and starts to heat the slab. Due to the thermo-optic effect, the transmission spectrum (Figure 1b) shifts to higher wavelength. As the slab continues to heat, the intersection of the shifted transmission curve with the dashed line (indicating the laser operating wavelength) traces out a Fano shape in time, evident in Figure 2e. Meanwhile, the absorption spectrum shifts in a similar fashion. While the absorption is initially low at the laser wavelength, the rightward shift causes the value to peak when the resonance of the slab crosses the laser wavelength. The large absorption at the crossing is responsible for the sudden temperature jump observed in Figure 2b.

We define the thermal response time as the elapsed time between laser turn-on and the sudden temperature rise. The thermal response time of our system can be tuned in several ways. First, increasing the laser power shortens the response time, as seen in Figure 2a,c,e. Second, decreasing the initial detuning of the laser from the resonance shortens the response time, since the initial absorption is increased and the heating time is reduced. Third, reducing the conductivity or the effective heat capacity of the photonic-crystal slab decreases the response time. The response time of the device can also be tailored by altering the beam waist. A tightly confined laser beam will shorten the response time, due to the increase in the local heating rate.

To investigate the time-dependent response experimentally, we fabricated and characterized a free-standing, silicon photonic-crystal membrane. Our fabrication procedure is described in detail in ref 28. The fabricated structure has a thickness of 340 nm, a lattice constant of 470 nm, and a hole diameter of 160 nm, as in the simulations above. We characterized the transmission spectrum of the device using a broadband white-light source and a spectrometer (Ocean Optics USB 4000). The measured transmission spectrum is depicted in Figure 3a. A resonant wavelength of 968 nm and a quality factor of 170 were obtained by fitting the transmission line shape to a Fano formula. The measured quality factor is

DOI: 10.1021/acsphotonics.5b00521
ACS Photonics 2015, 2, 1681−1685

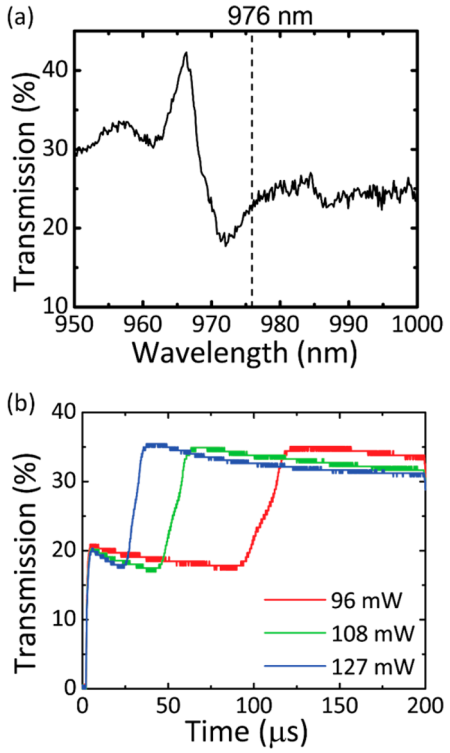

Figure 3. (a) Transmission spectrum of the fabricated device. (b) Transmission change as a function of time.

less than the simulated structure. We attribute the reduction to the finite numerical aperture of the 10× objectives (Mitutoyo NIR MPlan Apo) used to focus the incident beam on the sample (80 μm beam diameter) and collect the transmitted beam.

To measure the time-dependent, nonlinear response, we illuminated the sample with a near-infrared diode laser operating at 976 nm. The laser, pigtailed with a single-mode fiber, is passed through a 19 mm lens and focused through the objective onto the sample. This results in a Gaussian beam with a spot size of 10 μm on the sample. The laser output is modulated using a laser diode controller (Thorlabs) using a square pulse with modulation frequency of 1 Hz and 20% duty cycle. The rise time of the laser pulse is approximately 1 μs. The transmitted beam collected by the objective is fed to a fiber-coupled trans-impedance amplifier (Thorlabs) with a response time on the order of a few picoseconds.

The temporal response of the transmitted pulse through the photonic-crystal slab is shown in Figure 3b. For each power level, there is a large transmission jump between approximately 17% and 35%. The shape of the transmission curve (decreasing, increasing, then decreasing) coincides with the trend expected from shifting the transmission spectrum in Figure 3a to the right across the operating wavelength (dashed line). As the power is increased, the transmission jump shifts to shorter times, in agreement with the prediction in Figure 2e.

Several differences are observed between experiment and theory. First, the time-dependent transmission response is not as sharp as in simulations. The transmission jump occurs over 20 μs, compared to 1 μs in the simulation. This can primarily be attributed to the lower quality factor of the resonance. Additionally, the simulation did not include the increase in the absorption coefficient of silicon with temperature. This effect tends to lower the quality factor of the mode with increasing power. It causes the maximum transmission value observed in the temporal response of transmission (36%; Figure 3b) to be lower than the maximum value in the transmission spectrum (40%; Figure 3a). Second, the observed response time is longer than in simulation. This may result from differences in the value of thermal conductivity in simulation and experiment. However, the overall qualitative trends show good agreement between simulation and experiment.

We used the spectral shift in a monitored wavelength range[23] to estimate the steady-state temperature rise in the sample. Figure 4 shows the transmission spectrum of the device at

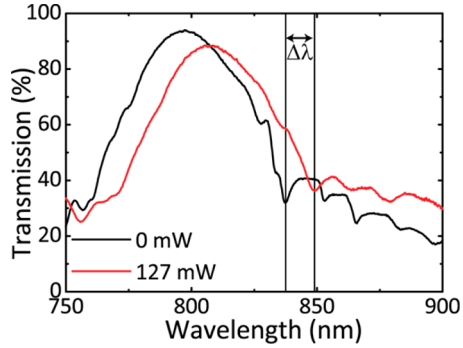

Figure 4. Spectral shift in the monitor wavelength range as a function of incident laser power.

lower wavelengths, e.g., below 976 nm. For a laser power of 127 mW (red line), the resonance dip at 837.5 nm shifts 11.5 nm to the right, relative to the spectrum for 0 mW. We estimate the temperature rise from the formula $\Delta T \approx (\Delta\lambda/\lambda)(n/(\partial n/\partial T))$, where $\Delta\lambda$ is the spectral shift. At a steady-state power of 127 mW, the estimated temperature rise was 168 K.

To confirm that our devices did not undergo any structural damage due to this large temperature rise, we performed measurements similar to Figure 3b multiple times and verified that there was only minimal run-to-run variability.

In addition to absorptive heating, free-carrier dispersion, Kerr nonlinearities, and two-photon absorption can affect the transmission spectrum.[29] However, Kerr nonlinearities and two-photon absorption are both third-order effects and should be minimal relative to linear absorption. Free-carrier dispersion produces a spectral blue shift. From Figure 4, we observe that the total spectral shift is toward the red, indicating that absorptive heating dominates over free-carrier dispersion.

In conclusion, we have introduced a novel nanoheater structure based on a nanopatterned silicon membrane. Heating occurs due to absorption enhancement in a guided resonance mode. We show theoretically that the temperature in the membrane jumps suddenly as a function of time. The onset of the jump can be tuned with laser power. Experimentally, we have observed a signature of the temperature rise via time-dependent optical transmission measurements. In these experiments, we operated at a wavelength of 976 nm. By adjusting the diameter and spacing of holes in the membrane, it is possible to shift the position of the resonance mode for operation at other laser wavelengths. Any wavelength within the 800−1100 nm range will allow the direct absorption of silicon to be used for heating. The sudden heater device presented here will open up a range of new nanoscale thermal applications, particularly in chemical and biological lab-on-a-chip experiments.

DOI: 10.1021/acsphotonics.5b00521
ACS Photonics 2015, 2, 1681−1685

AUTHOR INFORMATION

Corresponding Author

*E-mail: povinell@usc.edu.

Notes

The authors declare no competing financial interest.

ACKNOWLEDGMENTS

This work was supported by a National Science Foundation CAREER Award under Grant No. 0846143. Computational resources were provided by the University of Southern California Center for High-Performance Computing and Communications (www.usc.edu/hpcc). The authors thank Ahmed Morsy for his active participation in technical discussions and support with the experiments.

REFERENCES

(1) Baffou, G.; Quidant, R. Thermo-plasmonics: using metallic nanostructures as nano-sources of heat. *Laser & Photonics Reviews* **2013**, *7* (2), 171−187.

(2) Richardson, H. H.; Carlson, M. T.; Tandler, P. J.; Hernandez, P.; Govorov, A. O. Experimental and theoretical studies of light-to-heat conversion and collective heating effects in metal nanoparticle solutions. *Nano Lett.* **2009**, *9* (3), 1139−1146.

(3) Baffou, G.; Girard, C.; Quidant, R. Mapping heat origin in plasmonic structures. *Phys. Rev. Lett.* **2010**, *104* (13), 136805.

(4) Ma, H.; Tian, P.; Pello, J.; Bendix, P. M.; Oddershede, L. B. Heat Generation by Irradiated Complex Composite Nanostructures. *Nano Lett.* **2014**, *14* (2), 612−619.

(5) Liu, G. L.; Kim, J.; Lu, Y.; Lee, L. P. Optofluidic control using photothermal nanoparticles. *Nat. Mater.* **2006**, *5* (1), 27−32.

(6) Donner, J. S.; Baffou, G.; McCloskey, D.; Quidant, R. Plasmon-assisted optofluidics. *ACS Nano* **2011**, *5* (7), 5457−5462.

(7) Fang, Z.; Zhen, Y.-R.; Neumann, O.; Polman, A.; Garcia de Abajo, F. J.; Nordlander, P.; Halas, N. J. Evolution of light-induced vapor generation at a liquid-immersed metallic nanoparticle. *Nano Lett.* **2013**, *13* (4), 1736−1742.

(8) Gobin, A. M.; Lee, M. H.; Halas, N. J.; James, W. D.; Drezek, R. A.; West, J. L. Near-infrared resonant nanoshells for combined optical imaging and photothermal cancer therapy. *Nano Lett.* **2007**, *7* (7), 1929−1934.

(9) Qin, Z.; Bischof, J. C. Thermophysical and biological responses of gold nanoparticle laser heating. *Chem. Soc. Rev.* **2012**, *41* (3), 1191−1217.

(10) Stehr, J.; Hrelescu, C.; Sperling, R. A.; Raschke, G.; Wunderlich, M.; Nichtl, A.; Heindl, D.; Karzinger, K.; Parak, W. J.; Klar, T. A. Gold nanostoves for microsecond DNA melting analysis. *Nano Lett.* **2008**, *8* (2), 619−623.

(11) Auguie, B.; Barnes, W. L. Collective resonances in gold nanoparticle arrays. *Phys. Rev. Lett.* **2008**, *101* (14), 143902.

(12) Chu, Y.; Schonbrun, E.; Yang, T.; Crozier, K. B. Experimental observation of narrow surface plasmon resonances in gold nanoparticle arrays. *Appl. Phys. Lett.* **2008**, *93* (18), 181108.

(13) Chen, X.; Chen, Y.; Yan, M.; Qiu, M. Nanosecond photothermal effects in plasmonic nanostructures. *ACS Nano* **2012**, *6* (3), 2550−2557.

(14) Baffou, G.; Berto, P.; Bermúdez Ureña, E.; Quidant, R.; Monneret, S.; Polleux, J.; Rigneault, H. Photoinduced heating of nanoparticle arrays. *ACS Nano* **2013**, *7* (8), 6478−6488.

(15) Adleman, J. R.; Boyd, D. A.; Goodwin, D. G.; Psaltis, D. Heterogenous catalysis mediated by plasmon heating. *Nano Lett.* **2009**, *9* (12), 4417−4423.

(16) Cao, L.; Barsic, D.; Guichard, A.; Brongersma, M. Plasmon-Assisted Local Temperature Control to Pattern Individual Semiconductor Nanowires and Carbon Nanotubes. *Nano Lett.* **2007**, *7*, 3523−3527.

(17) Zhu, M.; Baffou, G.; Meyerbroker, N.; Polleux, J. Micropatterning thermoplasmonic gold nanoarrays to manipulate cell adhesion. *ACS Nano* **2012**, *6* (8), 7227−7233.

(18) Miao, X.; Wilson, B. K.; Lin, L. Y. Localized surface plasmon assisted microfluidic mixing. *Appl. Phys. Lett.* **2008**, *92* (12), 124108.

(19) Smith, A. M.; Mancini, M. C.; Nie, S. Bioimaging: Second window for in vivo imaging. *Nat. Nanotechnol.* **2009**, *4* (11), 710−711.

(20) Fan, S.; Joannopoulos, J. Analysis of guided resonances in photonic crystal slabs. *Phys. Rev. B: Condens. Matter Mater. Phys.* **2002**, *65* (23), 1−8.

(21) Crozier, K. B.; Lousse, V.; Kilic, O.; Kim, S.; Fan, S.; Solgaard, O. Air-bridged photonic crystal slabs at visible and near-infrared wavelengths. *Phys. Rev. B: Condens. Matter Mater. Phys.* **2006**, *73*, 115126.

(22) Lin, C.; Povinelli, M. L. Optical absorption enhancement in silicon nanowire arrays with a large lattice constant for photovoltaic applications. *Opt. Express* **2009**, *17*, 19371−19381.

(23) Biswas, R.; Povinelli, M. L. Photonic surfaces for designable nonlinear power shaping. *Appl. Phys. Lett.* **2015**, *106* (6), 061110.

(24) Chan, D. L. C.; Celanovic, I.; Joannopoulos, J. D.; Soljacic, M. Emulating one-dimensional resonant Q-matching behavior in a two-dimensional system via Fano resonances. *Phys. Rev. A: At., Mol., Opt. Phys.* **2006**, *74* (6), 064901.

(25) Fan, S.; Suh, W.; Joannopoulos, J. D. Temporal coupled-mode theory for the Fano resonance in optical resonators. *J. Opt. Soc. Am. A* **2003**, *20* (3), 569−572.

(26) Soljacic, M.; Lidorikis, E.; Hau, L. V.; Joannopoulos, J. D. Enhancement of microcavity lifetimes using highly dispersive materials. *Phys. Rev. E* **2005**, *71* (2), 026602.

(27) Tang, J.; Wang, H.; Lee, D. H.; Fardy, M.; Huo, Z.; Russell, T. P.; Yang, P. Holey Silicon as an Efficient Thermoelectric Material. *Nano Lett.* **2010**, *10*, 4279−4283.

(28) Lin, C.; Martínez, L.; Povinelli, M. Fabrication of transferrable, fully suspended silicon photonic crystal nanomembranes exhibiting vivid structural color and high-Q guided resonance. *J. Vac. Sci. Technol. B* **2013**, *13*, 050606-1−050606-5.

(29) Uesugi, T.; Song, B. S.; Asano, T.; Noda, S. Investigation of optical nonlinearities in an ultra-high-Q Si nanocavity in a two-dimensional photonic crystal slab. *Opt. Express* **2005**, *14*, 377−386.

DOI: 10.1021/acsphotonics.5b00521
ACS Photonics 2015, 2, 1681−1685